Hindawi Publishing Corporation
Journal of Nanomaterials
Volume 2011, Article ID 523638, 6 pages
doi:10.1155/2011/523638

Research Article

Fluoride Nanoscintillators

Luiz G. Jacobsohn,[1] Kevin B. Sprinkle,[1] Steven A. Roberts,[1] Courtney J. Kucera,[1] Tiffany L. James,[1] Eduardo G. Yukihara,[2] Timothy A. DeVol,[3] and John Ballato[1]

[1] *Center for Optical Materials Science and Engineering Technologies (COMSET), School of Materials Science and Engineering, Clemson University, Clemson, SC 29634, USA*
[2] *Physics Department, Oklahoma State University, Stillwater, OK 74078, USA*
[3] *Department of Environmental Engineering and Earth Sciences, Clemson University, Clemson, SC 29625-6510, USA*

Correspondence should be addressed to Luiz G. Jacobsohn, luiz@clemson.edu

Received 10 May 2010; Revised 23 July 2010; Accepted 28 September 2010

Academic Editor: Quanqin Dai

A preliminary investigation of the scintillation response of rare earth-doped fluoride nanoparticles is reported. Nanoparticles of $CaF_2:Eu$, $BaF_2:Ce$, and $LaF_3:Eu$ were produced by precipitation methods using ammonium di-*n*-octadecyldithiophosphate (ADDP) as a ligand that controls growth and lessens agglomeration. The structure and morphology were characterized by means of X-ray diffraction and transmission electron microscopy, while the scintillation properties of the nanoparticles were determined by means of X-ray and ^{241}Am irradiation. The unique aspect of scintillation of nanoparticles is related to the migration of carriers in the nanoscintillator. Our results showed that even nanoparticles as small as ~4 nm in size effectively scintillate, despite the diffusion length of *e-h* pairs being considerably larger than the nanoparticles themselves, and suggest that nanoparticles can be used for radiation detection.

1. Introduction

Scintillators are luminescent materials that are used in the detection of ionizing radiation. Accordingly, they find use in a wide range of security, medical, industrial, and research applications. Since the discovery of scintillator $NaI:Tl$ in 1948, there has been continuous interest and investment in new materials, and, as a result, hundreds of scintillators are known today [1–7]. Some of the most used scintillators are alkali, alkali-earth, and rare earth (RE) halides, including $NaI:Tl$, $LiI:Eu$, $BaF_2(:Ce)$, $CaF_2:Eu$, CeF_3, and $LaBr_3:Ce$. Unfortunately, many of these materials are hygroscopic, which impose severe limitations on their synthesis and use.

Over the past 10 years, there has been significant interest in the investigation and evaluation of the performance of nanoscale materials, with virtually all classes of materials having been prepared as nanoparticles, particularly luminescent ones [8–14]. Nanoparticles are generally defined as having sizes that range from 1 to 100 nm and consequently have high surface-to-volume ratios. The relative dominance of surface atoms in nanoparticles often allows for property manipulation. For example, Stouwdam and van Veggel [15] and Kömpe et al., [16] reported a substantially increased quantum yield from RE-doped nanoparticles following surface modifications, while Cooke et al. observed significant changes in the luminescence lifetime of $Y_2SiO_5:Ce$ nanoparticles dispersed in different liquids [17, 18]. To date, the investigation of luminescent nanoparticles has focused mostly on quantum dots for lighting and display applications, while their application as scintillators is essentially unexplored [19–25]. Nanoparticles correspond to a new realm of opportunity for scintillation technologies, and this work provides a preliminary investigation of the scintillation response of RE-doped fluoride nanoparticles.

Scintillation corresponds to the emission of light upon excitation due to ionizing radiation, and scintillation performance is mainly characterized by luminosity, speed (lifetime), and emission wavelength, with ruggedness, radiation resistance, and thermal and chemical stability being important characteristics of the scintillator material as well. Scintillation efficiency, η, can be described by the combination of three processes: conversion, β, transfer, Q, and luminescence, S, summarized in the relation, $\eta = \beta SQ$ [26] and discussed in detail below.

The first process corresponds to how efficiently the energy of the incoming radiation is used to produce electron-hole (*e-h*) pairs. For gamma-rays, β is commonly estimated by dividing the energy of the gamma-ray by 2 to 2.5 times the value of the bandgap energy. Once created, free electrons and holes migrate through the lattice of the scintillator material. While still energetic, they can ionize other atoms and the new free electrons can further ionize other atoms, generating a cascade. Through numerous inelastic interactions with bound electrons, they lose energy and eventually become incapable of creating further ionization. The duration of this process is estimated to be 10^{-15} to 10^{-13} s and generates conduction band electrons, valence band holes, excitons, and plasmons. Once below the ionization threshold, these free electrons and holes lose enough energy to strongly interact with the vibrations of the lattice (electron-phonon interactions) and thermalize within 10^{-12} to 10^{-11} s, moving to the bottom of the conduction band and to the top of the valence band, respectively. Typically, *e-h* pairs have diffusion length of about 100 nm in ionic crystals [27].

During this migration through the lattice, a fraction of the *e-h* pairs is lost, either trapped or recombined nonradiatively at quenching centers, resulting in a decrease in the number of pairs available to produce luminescence. Only those pairs that reach the luminescent centers contribute to scintillation, and the efficiency of this process is given by *S*. The remaining *e-h* pairs that recombine at the luminescence centers generate scintillation, and the intrinsic efficiency of the radiative recombination at the luminescent center is quantified by *Q*. Table 1 illustrates these quantities for some bulk fluoride crystals, together with their luminosity [26].

Moreover, a few RE-doped single crystal lanthanum fluoride scintillators have been previously investigated. LaF3 : Ce is a fast scintillator, with a reported luminosity of 2200 photons/MeV at 10% CeF3 doping [28], and LaF3 : Nd shows weak scintillation of 270 photons/MeV at 173 nm [29]. While the choice of host and dopant determines the efficiency of the conversion and luminescence processes, the unique aspect of scintillation in nanoparticles is related to the migration of the carriers through the nanoscintillator.

2. Experimental Procedures

2.1. Synthesis of Nanoparticles. Solution precipitation takes advantage of the solubility of certain compounds to promote chemical reactions and the formation of precipitates, which, in our case, are the nanoparticles. The solubility of a substance corresponds to its ability to dissolve into a homogeneous solution in presence of a solvent. When dissolution occurs, molecules of the solvent arrange and bond themselves around the molecules of the solute, generating heat, increasing entropy, and making the solution more thermodynamically stable than the solute alone. Several different species can be formed in the solution, with the solubility and the composition of its soluble components depending on the pH. The chemical properties of the solvent and solute, such as hydrogen bonding, dipole moment, and polarizability play major roles in this process. Most nitrates, sulfates, acetates, chlorides, bromides, iodides, alkali metals, and NH_4 compounds are soluble in water and can be used as precursors, while carbonates, sulfites, sulfides, phosphates, hydroxides, and oxides are insoluble. Synthesis of RE-doped fluoride nanoparticles was carried out by means of a modified solution precipitation method, where soluble metal nitrates ($Ca(NO_3)_2 \cdot 4H_2O$ (Fisher, 99.9%), $Eu(NO_3)_3 \cdot 6H_2O$ (Alfa Aesar, 99.9%), $Ba(NO_3)_2$ (Fisher, reagent grade), $Ce(NO_3)_3 \cdot 6H_2O$ (Acros Organic, 99.5%), and $La(NO_3)_3 \cdot 6H_2O$ (Aldrich, 99.99%)), and ammonium fluoride (Acros Organic, >98%) were used as the precursors. The solubility of a substance is further affected by the temperature and the nature of the solvent, and also on the presence of other substances dissolved in the solvent, particularly complex-forming anions (ligands). Two precursor solutions were used. One of them, contained NH_4F, the source of fluorine, and the ligand ammonium di-*n*-octadecyldithiophosphate (ADDP) in 1 : 1 ethanol : water at 75°C. The other solution contained the nitrates dissolved in water and was the source of the host and dopant metals.

Solvents can affect the solubility, stability, and reaction rates, allowing for thermodynamic and kinetic control over a chemical reaction. The polarity, dipole moment, polarizability, and hydrogen bonding of a solvent determine the types of compounds it is able to dissolve and the solvents and other liquid compounds it is miscible in. Generally, polar solvents dissolve polar compounds, and nonpolar solvents dissolve nonpolar compounds. Further, the choice of the solvent should take into account the reaction mechanism. Protic solvents like water solvate anions via hydrogen bonding, favoring the dissociative reaction mechanism, while aprotic solvents such as acetone or dichloromethane solvate cations via dipole interaction, favoring the interchange mechanism.

Of particular interest is the use of ligands during the synthesis of nanoparticles to control growth, avoid particle agglomeration, and provide dispersability in organic solvents. A ligand is an ion or molecule that bonds itself to a metal atom forming covalent or ionic bonds; chelation occurs when more than one chemical bond is formed with the central metal ion. Ligands also can be used as a "capping" agent to inactivate the metal so that it cannot react with other elements or ions to produce precipitates. In this work, the ligand ADDP is used in order to control growth and to avoid agglomeration of nanoparticles, as already has been demonstrated for the synthesis of other nanomaterials [15, 30–36]. ADDP was synthesized as follows [30]. P_2S_5 (0.02 mol) and octadecanol (0.07 mol) were heated at 75°C for 3 hours, and the resulting suspension cooled to room temperature at which point dichloromethane was added to solution, followed by filtration. The solvent was evaporated, the residue added into hexane, and ammonia was bubbled through the solution. The resulting precipitate was separated by filtration, washed with hexane, and dried. Water was purified using a Nanopure Diamond purification system from Barnstead International.

The synthesis of CaF_2 : Eu, BaF_2 : Ce, and LaF_3 : Eu nanoparticles consisted of dropwise addition of the nitrate solution into the fluorinated solution while stirring to form the nanoparticles in suspension. Rare earth doping levels

Table 1: Parameters relevant to the scintillation performance of selected fluoride scintillators.

Scintillator	Bandgap (eV)	β	Q	S	η	Luminosity (photons/MeV)
CeF_3	10.4	0.61	1.0	0.13	0.08	3200
$Ce_{0.5}La_{0.5}F_3$	10.4	0.61	1.0	0.16	0.1	4000
CaF_2 : Eu	12.2	0.63	1.0	~1	0.6	24000
BaF_2 (@310 nm)	10.6	<0.72	~1	>0.33	0.24	9950

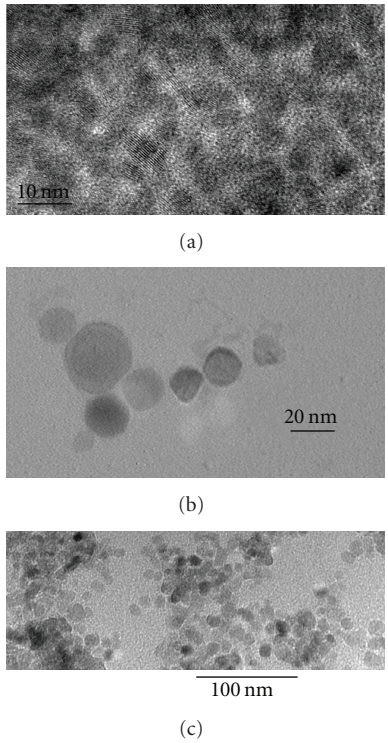

Figure 1: Selected TEM images of fluoride nanoscintillators: (a) LaF_3 : Eu, (b) BaF_2 : Ce, and (c) CaF_2 : Eu.

were 3 mol% for hosts CaF_2 and BaF_2 and 1 mol% for LaF_3. The final solution is stirred for 10 minutes and then cooled down to room temperature. Further, the precipitates were cleaned by washing in ethanol and water, followed by dispersion in dichloromethane (Acros, anhydrous, AcroSeal, 99.9%) and precipitation with the addition of 20 mL of ethanol. The resultant powder was dried for 2 days over P_2O_5 in a desiccator. The nanoparticles could be dispersed in tetrahydrofuran (Acros, anhydrous, AcroSeal, 99.9%) for characterization and testing [31].

2.2. Characterization. Samples in powder form were characterized for their morphology, structure, and scintillating properties. Morphological and particle size analysis was carried out using Hitachi H7600T transmission electron microscope with 120 kV acceleration voltage**.** Structural characterization was carried out through X-ray diffraction (XRD) measurements using a Scintag XDS 4000 diffractometer equipped with a Cu Kα source aiming at phase identification.

Scintillation response to two sources of ionizing radiation, namely, X-rays from Ag and the natural decay of ^{241}Am, was carried out using radioluminescence (RL) and differential pulse height distribution measurements, respectively. RL measurements used a 40 kV Bullet X-ray tube combined with a Ocean Optics USB-2000 miniature fiber optic spectrometer. The distance from the X-ray target to the sample was ~3 cm, and the X-ray tube was operated at 100 μA. For each measurement, a crucible with 57 mm^2 area was filled with nanopowder such that each sample had the same area exposed to the X-rays. Three measurements were carried for each sample yielding a reproducibility of about 10%–15%. No correction for differential light scattering, possibly arising from the different grain size distribution and powder packing in the crucibles, was attempted. Differential pulse height distribution measurements used a Hidex Triathler scintillation counter with a Hamamatsu R850-photomultiplier tube and a 1 μCi ^{241}Am (E_α = 5.5 MeV, E_γ = 60 keV) source. The Trialther was configured with logarithmic amplification to accentuate the difference in the differential pulse height spectra. In our measurements, the relative positions of the sample, detector and source were kept fixed, with the plated ^{241}Am source being suspended ~1 cm above power contained in a 3.7 mL borosilicate glass vial. The electronic noise background was determined by measuring an empty flask in identical conditions as the nanopowder sample.

3. Results and Discussion

The morphology of the nanoparticles, characterized by transmission electron microscopy (TEM), is shown in Figure 1. All the nanoparticles were found to have spheroidal shapes, and analysis of numerous images yielded average size and size distributions of each nanoscintillator. LaF_3 : Eu, CaF_2 : Eu, and BaF_2 : Ce nanoparticles were 4.4 ± 0.8 nm (size ± standard deviation), 10 ± 2 nm, and 18 ± 3 nm in size, respectively.

The structure of the nanoparticles was determined by XRD to be face-centered cubic for the alkali earth fluorides with space group Fm3m, in agreement with the International Centre for Diffraction Data powder diffraction files 35-0816 for CaF_2, and 04-0452 for BaF_2. The structure of LaF_3 : Eu nanoparticles was determined to be hexagonal with centrosymmetric space group $P\bar{3}c1$, in agreement with powder diffraction file 32-0483 [36].

The photoluminescence of LaF_3 : Eu nanoparticles and the cathodoluminescence of submicrometric particles have been reported before [15, 30, 35, 37, 38], while to the best

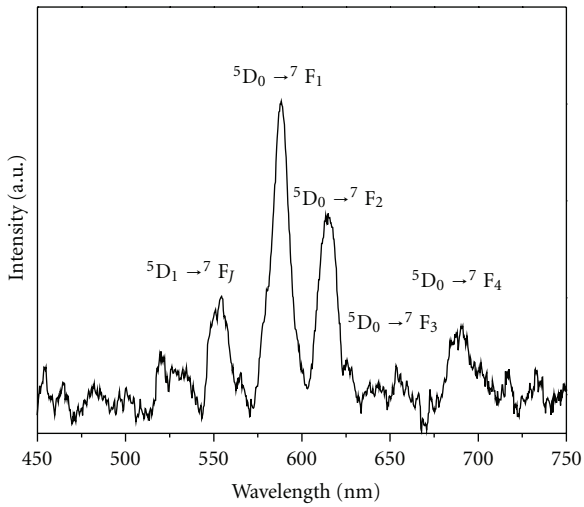

Figure 2: RL spectrum of LaF_3 : Eu nanoscintillator.

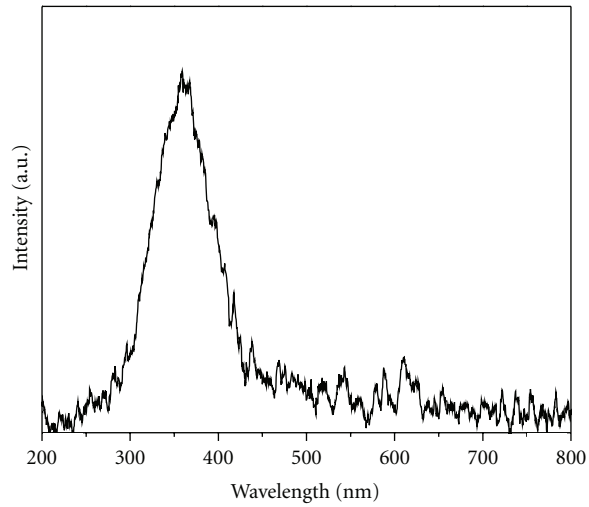

Figure 3: RL spectrum of BaF_2 : Ce nanoscintillator.

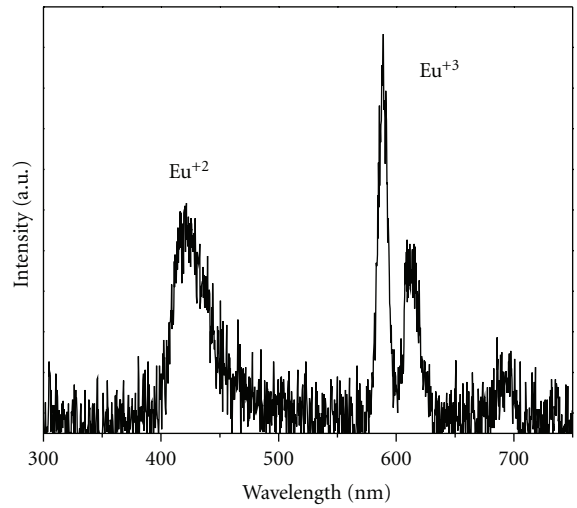

Figure 4: RL spectrum of CaF_2 : Eu nanoscintillator.

of our knowledge, the scintillation response of LaF_3 : Eu has not been investigated to date. Radioluminescence of these nanoscintillators under X-ray irradiation is presented in Figure 2, where a series of lines corresponding to the $^5D_{0,1} \rightarrow ^7F_J$ transitions can be seen. Emission at 588 nm dominates the spectrum, while the relatively high intensity of the hypersensitive transition $^5D_0 \rightarrow ^7F_2$ at 614 nm shows the existence of structural disorder that distort the inversion symmetry around the Eu^{3+} ions. Such a result is not surprising due to reduced dimensions of these nanoparticles and the consequent high fraction of atoms on the surface. It is well known that the loss of the three-dimensional crystalline periodicity of the atomic potential that exists inside a solid, and the lack of atoms to counter-balance and fully compensate chemical bonds and charge requirements result in structural modifications of the surface layer. The observation of intense emission due to electric dipole transitions of Eu^{3+} ions is ascribed to these modifications, similarly to the observations reported in [35].

Undoped BaF_2 is known to luminesce due to cross luminescence and self-trapped exciton recombination, while the presence of Ce is known to eliminate these recombination mechanisms [see [39] and references there in]. Vissert et al. carried out a detailed investigation of the effects of Ce doping on the luminescence of this scintillator, and identified three distinct luminescent centers related to the Ce dopant, named centers *Ce1*, *Ce2*, and *Ce3*, with the dominance of a given center depending on the Ce concentration. For concentrations around 1 mol% and higher, photoluminescence emission was observed in the approximate range of 330–370 nm and ascribed to center *Ce2*. Those authors also determined the photon output under X-ray excitation of BaF_2 : Ce for a wide range of Ce concentrations and based on their results the RL emission of a 3 mol% doped crystal is due to the *Ce2* center [39]. Figure 3 presents the RL spectrum of BaF_2 : Ce nanoparticles investigated in this work under X-ray irradiation. The nanoparticles scintillate at 350 nm, and no sign of the self-trapped exciton radiative recombination at around 300 nm was observed. Similar results were observed in 1 mol% Ce doped BaF_2 ceramics and crystals [40, 41].

The photoluminescence response of CaF_2 : Eu nanoparticles showed that emission is composed of electronic transitions from Eu^{2+} and Eu^{3+} ions. Similarly to the LaF_3:Eu nanoparticles, structural disorder manifested in terms of deviations from inversion symmetry around the Eu^{3+} ion made the hypersensitive transition $^5D_0 \rightarrow ^7F_2$ particularly intense [36]. Radioluminescence results are shown in Figure 4, where a broad band centered at 420 nm due to the emission of Eu^{+2}, and the emission lines in the 550–750 nm range due to the $^5D_1 \rightarrow ^7F_J$ transitions of Eu^{+3} can be observed. Similarly to LaF_3 : Eu, the relatively intense emission of the $^5D_1 \rightarrow ^7F_2$ transition at 611 nm shows the existence of structural disorder that distort the inversion symmetry around the Eu^{3+} ions.

The scintillation response of CaF_2 : Eu nanoparticles under ^{241}Am irradiation determined by means of differential pulse height distribution measurements is presented in

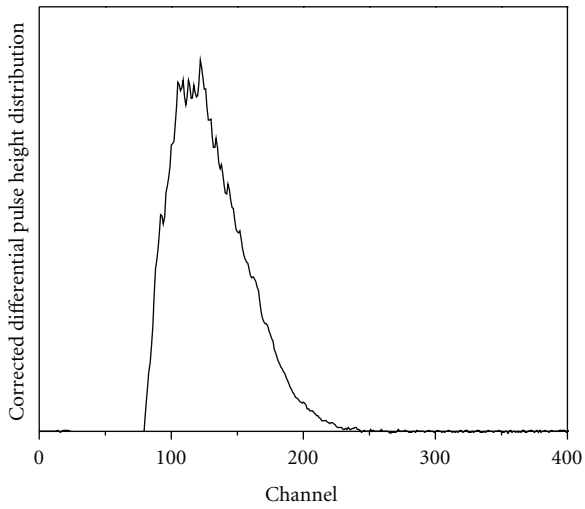

Figure 5: Corrected differential pulse height distribution measurement of CaF_2 : Eu nanoscintillator.

Figure 5 after the subtraction of the electronic noise, where a photopeak centered around channel 120 can be observed. This signal is due the irradiation of 5.5 MeV alpha particles from the ^{241}Am source, since shielding of the alpha particles resulted in no detectable net signal under the experimental conditions employed here. Under irradiation of X-rays and alpha particles, a great number of *e-h* pairs are formed. As discussed in the introduction, the migration of the *e-h* pairs through the scintillator is inherent to the scintillation mechanism and scintillation occurs when they recombine at the RE ions. The net scintillation intensity is determined by the competition between radiative recombination at the luminescence sites versus nonradiative recombination at quenching centers, particularly on the surface of the nanoparticles, and trapping of the carriers. Given the fact that the diffusion length of *e-h* pairs in the alkali halides is around 100 nm [42], and tens of nm in oxides and oxy-sulfides [43, 44], it is interesting to observe efficient scintillation when the dimensions of the nanoparticles are considerably smaller than the diffusion length, concomitant to a relatively high probability of nonradiative recombination on the surface of the nanoparticles. This result has relevant implications on the use of nanoparticles for radiation detection.

4. Summary and Conclusions

The use of luminescent nanoparticles as scintillators is a new field, and in this work, a preliminary survey of the scintillation response of fluoride nanoscintillators CaF_2 : Eu, BaF_2 : Ce, and LaF_3 : Eu was carried out using both X-rays and ^{241}Am sources. The unique aspect of scintillation in nanoparticles is related to the migration of the carriers through the nanoscintillator, and our results showed that even nanoparticles as small as ~4 nm in size effectively scintillate under irradiation. This is an interesting result given that the diffusion length of *e-h* pairs in many scintillators is determined to be in the range of tens to a 100 nm, and significant nonradiative recombination at the surface of the nanoparticles should be expected. These results also show that RE-doped fluoride nanoparticles can be used for radiation detection of a wide range of ionizing radiations, and that this topic is worth further consideration and deeper investigation.

Acknowledgments

The authors acknowledge the partial support of DTRA through Grant no. HDTRA1-08-1-0015 and DARPA through Grant no. N66001-04-1-8933.

References

[1] S. E. Derenzo, W. W. Moses, J. L. Cahoon, R. C. C. Perera, and J. E. Litton, "Prospects for new inorganic scintillators," *IEEE Transactions on Nuclear Science*, vol. 37, no. 1, pp. 203–208, 1990.

[2] G. Blasse, "Search for new inorganic scintillators," *IEEE Transactions on Nuclear Science*, vol. 38, no. 1, pp. 30–31, 1991.

[3] M. Ishii and M. Kobayashi, "Single crystals for radiation detectors," *Progress in Crystal Growth and Characterization of Materials*, vol. 23, pp. 245–311, 1992.

[4] G. Blasse, "Scintillator materials," *Chemistry of Materials*, vol. 6, no. 9, pp. 1465–1475, 1994.

[5] G. Blasse, "Luminescent materials: is there still news?" *Journal of Alloys and Compounds*, vol. 225, no. 1-2, pp. 529–533, 1995.

[6] S. E. Derenzo, M. J. Weber, E. Bourret-Courchesne, and M. K. Klintenberg, "The quest for the ideal inorganic scintillator," *Nuclear Instruments and Methods in Physics Research A*, vol. 505, no. 1-2, pp. 111–117, 2003.

[7] B. D. Milbrath, A. J. Peurrung, M. Bliss, and W. J. Weber, "Radiation detector materials: an overview," *Journal of Materials Research*, vol. 23, no. 10, pp. 2561–2581, 2008.

[8] H. Chander, "Development of nanophosphors—a review," *Materials Science and Engineering R: Reports*, vol. 49, no. 5, pp. 113–155, 2005.

[9] C. Li and J. Lin, "Rare earth fluoride nano-/microcrystals: synthesis, surface modification and application," *Journal of Materials Chemistry*, vol. 20, no. 33, pp. 6831–6847, 2010.

[10] C. Zhang, C. Li, C. Peng et al., "Facile and controllable synthesis of monodisperse CaF_2 and CaF_2:Ce^{3+}/Tb^{3+} hollow spheres as efficient luminescent materials and smart drug carriers," *Chemistry*, vol. 16, no. 19, pp. 5672–5680, 2010.

[11] C. Li, J. Yang, P. Yang, H. Lian, and J. Lin, "Hydrothermal synthesis of lanthanide fluorides LnF_3 (Ln = la to Lu) nano-/microcrystals with multiform structures and morphologies," *Chemistry of Materials*, vol. 20, no. 13, pp. 4317–4326, 2008.

[12] Z. Quan, D. Yang, P. Yang et al., "Uniform colloidal alkaline earth metal fluoride nanocrystals: nonhydrolytic synthesis and luminescence properties," *Inorganic Chemistry*, vol. 47, no. 20, pp. 9509–9517, 2008.

[13] C. Li, Z. Quan, J. Yang, P. Yang, and J. Lin, "Highly uniform and monodisperse β-$NaYF_4$:Ln^{3+} (Ln = Eu, Tb, Yb/Er, and Yb/Tm) hexagonal microprism crystals: hydrothermal synthesis and luminescent properties," *Inorganic Chemistry*, vol. 46, no. 16, pp. 6329–6337, 2007.

[14] Z. L. Wang, Z. W. Quan, P. Y. Jia et al., "A facile synthesis and photoluminescent properties of redispersible CeF_3, CeF_3:Tb^{3+}, and CeF_3:Tb^{3+}/LaF_3 (core/shell) nanoparticles," *Chemistry of Materials*, vol. 18, no. 8, pp. 2030–2037, 2006.

[15] J. W. Stouwdam and F. C. J. M. van Veggel, "Improvement in the luminescence properties and processability of LaF_3/Ln and $LaPO_4$/Ln nanoparticles by surface modification," *Langmuir*, vol. 20, no. 26, pp. 11763–11771, 2004.

[16] K. Kömpe, O. Lehmann, and M. Haase, "Spectroscopic distinction of surface and volume ions in cerium(III)- and terbium(III)-containing core and core/shell nanoparticles," *Chemistry of Materials*, vol. 18, no. 18, pp. 4442–4446, 2006.

[17] D. W. Cooke, J.-K. Lee, B. L. Bennett et al., "Luminescent properties and reduced dimensional behavior of hydrothermally prepared Y_2SiO_5: Ce nanophosphors," *Applied Physics Letters*, vol. 88, no. 10, Article ID 103108, 3 pages, 2006.

[18] R. E. Muenchausen, L. G. Jacobsohn, B. L. Bennett, E. A. McKigney, J. F. Smith, and D. W. Cooke, "A novel method for extracting oscillator strength of select rare-earth ion optical transitions in nanostructured dielectric materials," *Solid State Communications*, vol. 139, no. 10, pp. 497–500, 2006.

[19] W. Chen, G. Huang, H. Lu, D. E. McCready, A. G. Joly, and J.-O. Bovin, "Utilizing nanofabrication to construct strong, luminescent materials," *Nanotechnology*, vol. 17, no. 10, pp. 2595–2601, 2006.

[20] I. H. Campbell and B. K. Crone, "Quantum-dot/organic semiconductor composites for radiation detection," *Advanced Materials*, vol. 18, no. 1, pp. 77–79, 2006.

[21] S. E. Létant and T.-F. Wang, "Semiconductor quantum dot scintillation under γ-ray irradiation," *Nano Letters*, vol. 6, no. 12, pp. 2877–2880, 2006.

[22] E. A. McKigney, R. E. Del Sesto, L. G. Jacobsohn et al., "Nanocomposite scintillators for radiation detection and nuclear spectroscopy," *Nuclear Instruments and Methods in Physics Research A*, vol. 579, no. 1, pp. 15–18, 2007.

[23] J. A. Johnson, S. Schweizer, B. Henke et al., "Eu-activated fluorochlorozirconate glass-ceramic scintillators," *Journal of Applied Physics*, vol. 100, no. 3, Article ID 034701, 5 pages, 2006.

[24] Y. S. Zhao, Z. Yu, A. Douraghy, A. F. Chatziioannou, Y. Mo, and Q. Pei, "A facile route to bulk high-Z polymer composites for gamma ray scintillation," *Chemical Communications*, no. 45, pp. 6008–6010, 2008.

[25] E. A. Mckigney, R. E. Muenchausen, D. W. Cooke et al., "$LaFM_3$:Ce nanocomposite scintillator for gamma-ray detection," in *Hard X-Ray and Gamma-Ray Detector Physics IX*, vol. 6706 of *Proceedings of SPIE*, San Diego, Calif, USA, August 2007.

[26] A. Lempicki, A. J. Wojtowicz, and E. Berman, "Fundamental limits of scintillator performance," *Nuclear Instruments and Methods in Physics Research A*, vol. 333, no. 2-3, pp. 304–311, 1993.

[27] P. A. Rodnyi, *Physical Processes in Inorganic Scintillators*, CRC Press, Boca Raton, Fla, USA, 1997.

[28] W. W. Moses and S. E. Derenzo, "The scintillation properties of cerium-doped lanthanum fluoride," *Nuclear Instruments and Methods in Physics Research A*, vol. 299, no. 1–3, pp. 51–56, 1990.

[29] P. Dorenbos, J. T. M. de Haas, and C. W. E. van Eijk, "The intensity of the 173 nm emission of LaF_3: Nd^{3+} scintillation crystals," *Journal of Luminescence*, vol. 69, no. 4, pp. 229–233, 1996.

[30] J. W. Stouwdam, G. A. Hebbink, J. Huskens, and F. C. J. M. van Veggel, "Lanthanide-doped nanoparticles with excellent luminescent properties in organic media," *Chemistry of Materials*, vol. 15, no. 24, pp. 4604–4616, 2003.

[31] J. R. DiMaio, B. Kokuoz, T. L. James, and J. Ballato, "Structural determination of light-emitting inorganic nanoparticles with complex core/shell architectures," *Advanced Materials*, vol. 19, no. 20, pp. 3266–3270, 2007.

[32] J. R. DiMaio, C. Sabatier, B. Kokuoz, and J. Ballato, "Controlling energy transfer between multiple dopants within a single nanoparticle," *Proceedings of the National Academy of Sciences of the United States of America*, vol. 105, no. 6, pp. 1809–1813, 2008.

[33] J. R. DiMaio, B. Kokuoz, and J. Ballato, "White light emissions through down-conversion of rare-earth doped LaF_3 nanoparticles," *Optics Express*, vol. 14, no. 23, pp. 11412–11417, 2006.

[34] J. DiMaio, B. Kokuoz, T. L. James, T. Harkey, D. Monofsky, and J. Ballato, "Photoluminescent characterization of atomic diffusion in core-shell nanoparticles," *Optics Express*, vol. 16, no. 16, pp. 11769–11775, 2008.

[35] V. Sudarsan, F. C. J. M. van Veggel, R. A. Herring, and M. Raudsepp, "Surface Eu^{3+} ions are different than "bulk" Eu^{3+} ions in crystalline doped LaF_3 nanoparticles," *Journal of Materials Chemistry*, vol. 15, no. 13, pp. 1332–1342, 2005.

[36] L. G. Jacobsohn, C. J. Kucera, T. L. James et al., "Preparation and characterization of rare earth doped fluoride nanoparticles," *Materials*, vol. 3, pp. 2053–2068, 2010.

[37] D. Pi, F. Wang, X. Fan, M. Wang, and Y. Zhang, "Luminescence behavior of Eu^{3+} doped LaF_3 nanoparticles," *Spectrochimica Acta A*, vol. 61, no. 11-12, pp. 2455–2459, 2005.

[38] Z.-L. Wang, H. L. W. Chan, H.-L. Li, and J. H. Hao, "Highly efficient low-voltage cathodoluminescence of LaF_3: Ln^{3+} (Ln= Eu^{3+}, Ce^{3+}, Tb^{3+}) spherical particles," *Applied Physics Letters*, vol. 93, no. 14, Article ID 141106, 3 pages, 2008.

[39] R. Visser, P. Dorenbos, C. W. E. van Eijk, A. Meijerink, G. Blasse, and H. W. den Hartog, "Energy transfer processes involving different luminescence centres in BaF_2:Ce," *Journal of Physics: Condensed Matter*, vol. 5, no. 11, pp. 1659–1680, 1993.

[40] S. Kh. Batygov, L. S. Bolyasnikova, V. A. Demidenko et al., "BaF2:Ce^{3+} scintillation ceramics," *Doklady Physics*, vol. 53, no. 9, pp. 485–488, 2008.

[41] R. Visser, P. Dorenbos, C. W. E. van Eijk, R. W. Hollander, and P. Schotanus, "Scintillation properties of Ce^{3+} doped BaF_2 crystals," *IEEE Transactions on Nuclear Science*, vol. 38, no. 2, pp. 178–183, 1991.

[42] K. Schwartz, *Atomic Physics Methods in Modern Research*, Springer, Berlin, Germany, 1997.

[43] E. L. Benitez, D. E. Husk, S. E. Schnatterly, and C. Tarrio, "A surface recombination model applied to large features in inorganic phosphor efficiency measurements in the soft X-ray region," *Journal of Applied Physics*, vol. 70, no. 6, pp. 3256–3260, 1991.

[44] V. B. Mikhailik, H. Kraus, G. Miller, M. S. Mykhaylyk, and D. Wahl, "Luminescence of $CaWO_4$, $CaMoO_4$, and $ZnWO_4$ scintillating crystals under different excitations," *Journal of Applied Physics*, vol. 97, no. 8, Article ID 083523, 8 pages, 2005.